Journal of Magnetic Resonance 209 (2011) 227–232

Contents lists available at ScienceDirect

Journal of Magnetic Resonance

journal homepage: www.elsevier.com/locate/jmr

Variable radio frequency proton–electron double-resonance imaging: Application to pH mapping of aqueous samples

Olga V. Efimova, Ziqi Sun, Sergey Petryakov, Eric Kesselring, George L. Caia, David Johnson, Jay L. Zweier, Valery V. Khramtsov *, Alexandre Samouilov *

Davis Heart and Lung Research Institute, College of Medicine, The Ohio State University, OH 43210, USA

ARTICLE INFO

Article history:
Received 5 August 2010
Revised 8 December 2010
Available online 15 January 2011

Keywords:
Functional proton MRI
Free radicals
Variable radio frequency PEDRI
pH

ABSTRACT

Proton–electron double-resonance imaging (PEDRI) offers rapid image data collection and high resolution for spatial distribution of paramagnetic probes. Recently we developed the concept of variable field (VF) PEDRI which enables extracting a functional map from a limited number of images acquired at pre-selected EPR excitation fields using specific paramagnetic probes (Khramtsov et al., J. Magn. Reson. 202 (2010) 267–273). In this work, we propose and evaluate a new modality of PEDRI-based functional imaging with enhanced temporal resolution which we term variable radio frequency (VRF) PEDRI. The approach allows for functional mapping (e.g., pH mapping) using specifically designed paramagnetic probes with high quality spatial resolution and short acquisition times. This approach uses a stationary magnetic field but different EPR RFs. The ratio of Overhauser enhancements measured at each pixel at two different excitation frequencies corresponding to the resonances of protonated and deprotonated forms of a pH-sensitive nitroxide is converted to a pH map using a corresponding calibration curve. Elimination of field cycling decreased the acquisition time by exclusion periods of ramping and stabilization of the magnetic field. Improved magnetic field homogeneity and stability allowed for the fast MRI acquisition modalities such as fast spin echo. In total, about 30-fold decrease in EPR irradiation time was achieved for VRF PEDRI (2.4 s) compared with VF PEDRI (70 s). This is particularly important for in vivo applications enabling one to overcome the limiting stability of paramagnetic probes and sample overheating by reducing RF power deposition.

Published by Elsevier Inc.

1. Introduction

Magnetic resonance imaging (MRI) is a leading technique in visualization of anatomical structure based on abundance of NMR-sensitive nuclei, water protons, in living tissues. However MRI has limited functional resolution, in part due to overlap with endogenous NMR signals. Electron paramagnetic resonance (EPR), on the contrary, possesses a high functionality and signal specificity due to the lack of endogenous paramagnetic species. Nevertheless, functional EPR imaging, EPRI, suffers from a low penetration depth of the microwaves in aqueous samples, insufficient in vivo stability of available paramagnetic probes and a requirement of powerful field gradients and/or of extraordinary fast pulse techniques due to short relaxation time of the EPR probes. The latter also results in limited spatial resolution of EPRI.

Proton–electron double-resonance imaging (PEDRI) [1] or Overhauser-enhanced magnetic resonance imaging (OMRI) [2] is a technique that combines both, the functional resolution of EPR and spatial resolution of MRI. In this approach spatial distribution of the NMR signal is detected under condition of saturation of the electron spin system by radio frequency (RF) microwave irradiation. Significant enhancement of the NMR signal, with a theoretical maximum enhancement factor of 328, arises from transferring the polarization from free electron of the paramagnetic probe to the magnetically-coupled water protons. Comparison of the EPR *off* and EPR *on* MRI images gives spatial localization of the paramagnetic species [3–9]. Therefore, PEDRI inherently offers high spatial resolution and rapid image data collection.

A field-cycled mode (FC) PEDRI [10,11] was developed to reduce power deposition during the EPR irradiation for in vivo experiments and increase the contrast of the MRI image of paramagnetic probe distribution within a sample. Recently we developed a concept of variable field (VF) PEDRI [12] which allows for extracting spatially resolved functional information from a limited number of images acquired at pre-selected EPR excitation fields using specific paramagnetic probes.

* Corresponding authors. Address: Davis Heart and Lung Research Institute, The Ohio State University, 420 West 12th Ave., Room 611B, Columbus, OH 43210, USA (A. Samouilov).

E-mail addresses: valery.khramtsov@osumc.edu (V.V. Khramtsov), alex.samouilov@osumc.edu (A. Samouilov).

1090-7807/$ - see front matter Published by Elsevier Inc.
doi:10.1016/j.jmr.2011.01.011

In this work, we report the development of a new modality of functional imaging in living tissues, namely variable radio frequency (VRF) PEDRI, which allows for about 30-fold decrease in the acquisition time compared with that for VF PEDRI. This is particularly important for in vivo applications enabling one to overcome the limiting stability of paramagnetic probes and sample overheating by reduction of the RF power deposition.

2. Materials and methods

2.1. Paramagnetic probe

The pH-sensitive nitroxyl radical R1, 4-amino-2,2,5,5-tetramethyl-3-imidazoline-1-yloxy, was synthesized as previously described [13]. The structure of the radical is shown in Fig. 1.

2.2. Instrument

VRF PEDRI experiments were performed on a home-made imager/spectrometer [11]. This imager was primarily designed for field cycling experiments and is, therefore, equipped with additional parts of hardware which are not necessary for VRF PEDRI. These include a secondary electromagnet built into the gap of the primary 0.38 T clinical MRI magnet and field cancellation coils. Elimination of these parts for future projects will increase the gap in the magnet system and will make it possible to use conventional NMR gradients and gradient power supplies.

2.3. Magnet and magnet power supply

A water-cooled iron core Resonex 5000/Paradigm resistive magnet (Resonex Corp., Sunnyvale, CA) is used to generate the main vertical magnetic field with a gap of 50 cm between the magnet poles. High homogeneity of the NMR detection field required for low field experiments is achieved by a set of 24 active shims, providing a homogeneity of better than 50 ppm over a sample of size $50 \times 40 \times 40$ cm placed at its isocenter, and better than 20 ppm over a $25 \times 20 \times 20$ cm sample volume. Danfysik MPS 854/SYS 8000 power supply is used to power the magnet to establish a magnetic field up to 0.38 T. Current regulation of the magnetic field relies on the high precision manually adjustable reference voltage, providing stability better than 0.5 ppm/h of the current and, therefore, of the magnetic field.

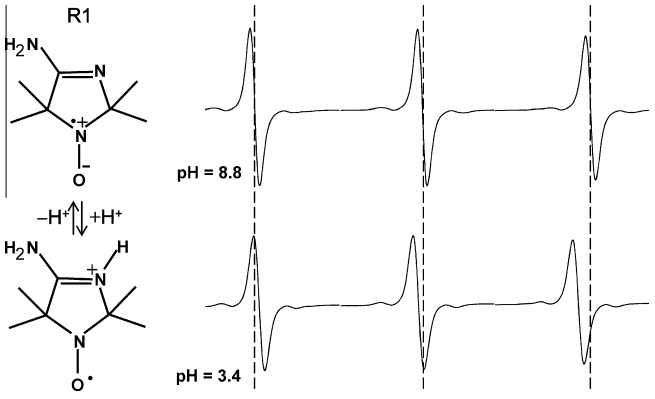

Fig. 1. The scheme of the reversible protonation of the imidazoline radical, R1 ($pK_a = 6.1$), and corresponding X-band EPR spectra of its protonated, RH^+, and unprotonated, R, forms. The preferable resonance structures are shown illustrating higher unpaired electron density on nitrogen atom N-1 in the unprotonated form. Protonation results in an EPR-detected difference in hyperfine splitting, a_N, and g-factor ($\Delta a_N = 0.8$ G and $\Delta g = 0.0002$) between R and RH^+ forms. A dotted line is extended from the center of each component of the top spectrum to aid the eye.

2.4. Resonators' assembly

EPR transmit system, surrounding NMR resonator, is based on a modified Alderman–Grant design resonator with capacitive coupling in combination with a typical solenoidal coil for the NMR channel [14]. NMR resonator is placed in closer proximity to the sample to maximize NMR sensitivity.

2.5. NMR console

Individual parts of the imaging system are controlled by a customized MRRS MR 5000 console (MR Solutions Inc., Surrey, UK), including gradient hardware, the RF system, field-cycling coils (which are not used for VRF PEDRI experiments), and the magnet shim coils. Console also provides image acquisition and post-processing.

2.6. Spin echo sequence and experimental parameters

A standard 2D fast spin echo (FSE) pulse sequence from MR Solutions Inc. was used for fixed-field PEDRI experiments (Fig. 2). The continuous wave (CW) EPR irradiation was turned on about 400 ms before the execution of the FSE pulse sequence and was kept on during the whole *k*-space coverage. Single slice images were typically acquired using the 2D FSE pulse sequence (TR = 500 ms, base TE = 19 ms, effective TE = 95 ms, views per segment = 16, slice thickness = 10 mm, FOV = 100×100 mm, matrix size = 64×64, number of average = 1, scan time = 2.4 s, the number of dummy scans = 4). Images in this work were acquired with EPR irradiation at $RF_1 = 560.3$ MHz and $RF_2 = 562.5$ MHz. Incident EPR RF power was 12 W. EPR resonator frequency was 561.4 MHz.

2.7. Phantom for pH calibration

Solutions of R1 in the concentration of 1 mM and 2 mM in 10 mM pyrophosphate buffer were titrated to the desired pH values. For measurement of a calibration curve the phantom samples (10 glass tubes, 400 μl volume, 32 mm long and 4 mm in diameter) filled with R1 solutions covering pH range from 4.1 to 8.2, were used.

2.8. MATLAB analysis

Data analysis was performed on MATLAB using a home designed code for image reconstruction. First, images acquired

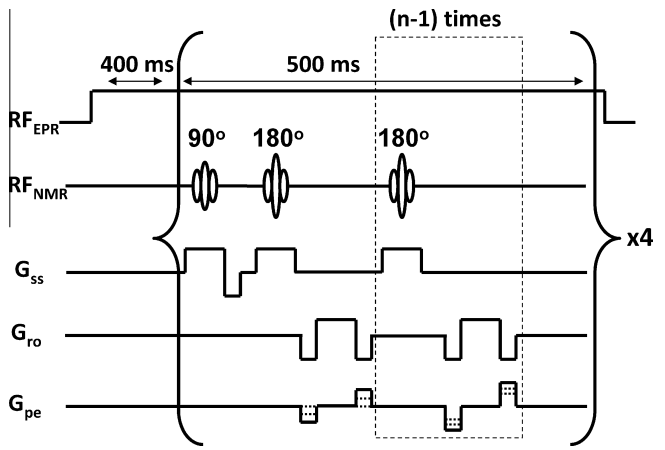

Fig. 2. 2D fast spin echo (FSE) pulse sequence, showing 2 out of 16 180° refocusing pulses. Number of echoes per RF excitation, $n = 16$; the number of RF excitations is 4.

without EPR irradiation were subtracted from images obtained at two EPR frequencies and, as explained above, the resulting images were divided pixel by pixel. Within an individual tube with known pH, only significant pixels, with the signal enhancement exceeding 7-fold, were used for calculating the averaged ratio which was plotted as a function of pH.

3. Results

3.1. Variable radio frequency PEDRI concept

PEDRI and dynamic nuclear polarization are two approaches based on Overhauser-enhanced NMR signal detection which provide complementary information on spatial distribution and EPR spectral parameters of paramagnetic probes, correspondingly. VRF PEDRI approach is intended to obtain both spatial and specific spectral information with a minimal number of PEDRI images acquired at pre-selected EPR frequencies.

The concept of VRF PEDRI, demonstrated by using it to do pH mapping using pH-sensitive nitroxide R1, is illustrated in Fig. 3. Protonation of the pH-sensitive nitroxyl radical results in a 0.8 G shift of its high-field spectral component due to corresponding decrease of nitrogen hyperfine splitting (please see Fig. 1). This shift is equal to 2.2 MHz difference at fixed field experiments performed at 200 G field which corresponded to proton MR frequency of 783.3 kHz. EPR irradiation was performed at two frequencies satisfying the resonance condition of pH sensitive high-field component in protonated or deprotonated form. EPR irradiation frequencies were initially calculated from experimentally obtained DNP spectra of completely protonated and deprotonated samples [12]. Additionally, these frequencies were fine tuned to maximize DNP enhancements of completely protonated and deprotonated samples. Chosen 560.3 MHz and 562.5 MHz frequencies corresponded to maximum enhancements of the protonated and deprotonated form respectively. EPR resonator was tuned to 561.4 MHz to be equally distanced from predetermined irradiation frequencies.

Two MRI images are acquired with irradiation of the sample at two EPR radio frequencies, RF_i ($i = 1, 2$). Differences between the signal intensities at each pixel of the MRI images with EPR irradiation *on* and *off*, $I(RF_i)$, are calculated for both EPR frequencies.

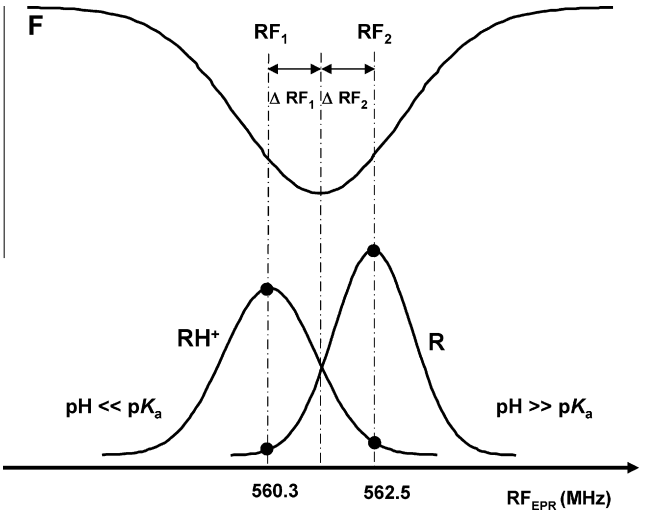

Fig. 3. Schematic representation of the variable frequency PEDRI experiment is demonstrated by using it to do pH mapping using pH-sensitive nitroxide R1. $\mathbf{RF_i}$ ($i = 1, 2$), two EPR radio frequencies, corresponding to the centers of the high field EPR component of the protonated, RH^+, and unprotonated, R, forms of the radical, respectively. **F**, the return loss of the EPR resonator. Resonator is tuned to the frequency equally distant from $\mathbf{RF_1}$ and $\mathbf{RF_2}$, so that $\Delta\mathbf{RF_1} = \Delta\mathbf{RF_2}$.

The map of the ratio $I(RF_1)/I(RF_2)$ is constructed and then converted to a pH map. In general, the ratio $I(RF_1)/I(RF_2)$ is determined by the contributions of the RH^+ and R forms in the signal intensity differences, $I(RF_1)$ and $I(RF_2)$, and therefore is directly related to the local acidity ($[RH^+]/[R] = [H^+]/K_a$) allowing for pH mapping of the sample. In practice, calibration of the method is required and can be done using phantom samples with known pH as shown below. One of the advantages of the VRF PEDRI over VF PEDRI [12] is the acquisition at a fixed magnetic field; this results in elimination of ramping and stabilization times. An improved magnetic field homogeneity and stability allows for the fast spin echo sequence and decreasing the acquisition time by more than order of magnitude.

3.2. Calibration of the VRF PEDRI approach for pH mapping

For construction of a calibration curve VRF PEDRI experiments have been performed using a 10-tube phantom filled with H_2O or 1 and 2 mM aqueous solutions of R1 with different values of pH ranging from 4.1 to 8.2 (Fig. 4A). pH values of the phantom tubes were selected to be tightly clustered around pK_a of R1 radical, where the determination of pH is more reliable. EPR irradiation was performed at two pre-selected EPR frequencies, $RF_1 = 560.3$ MHz (Fig. 4B) and $RF_2 = 562.5$ MHz (Fig. 4C) corresponding to the centers of the high field EPR component of the RH^+ and R forms of the R1 radical. Offset from the EPR resonator central frequency leads to reduced resonator efficiency. Therefore, to maintain the same EPR power in both acquisitions, the EPR resonator was tuned to 561.4 MHz which is equally distant from RF_1 and RF_2. Q factor of the sample-loaded resonator is 200 meaning that a shift from the central frequency by 1.12 MHz leads to a decrease in the EPR RF irradiation power by less than 10% within the sample. Fast spin echo sequence has been applied with acquisition time 2.4 s for each image.

The obtained images of the phantom are shown in Fig. 4. When acquired at RF_1 (Fig. 4B), signals from the upper left tube filled with the most acidic solution and bottom right tube with the most alkaline solution demonstrated the highest and lowest enhancements, about 25 and 15, correspondingly. The situation is reversed for the image acquired at RF_2 (Fig. 4C). The tube with water alone is not visible on the either image due to lower intensity compared to signals from tubes containing paramagnetic probe. While spatial mapping of regions containing paramagnetic probe and enhanced by EPR RF irradiation is not a problem at our experimental setting, obtaining anatomical information of non-enhanced regions is more difficult at low field MRI. If anatomical information is necessary, multiple acquisitions of not enhanced sample can overcome this limitation.

Simultaneous presence of nine tubes with different pH values in one phantom allows for obtaining a pH calibration curve from two acquisitions taking in total only 4.8 s of EPR RF irradiation time. Signal enhancement depends on the concentration of the paramagnetic probe, being directly proportional to the probe concentration in a millimolar range for the nitroxides [11]. To prove that VRF PEDRI method of pH detection is ratiometric, the calibration curves were obtained using the phantoms constructed from the tubes filled with 1 mM and 2 mM concentrations of the radical R1. The corresponding dependencies of intensities ratio $I(RF_1)/I(RF_2)$ on pH are shown in Fig. 5. Each point on the graphs corresponds to an averaged value of the ratios within the individual tube, calculated for each pixel of the image (see Section 2 for details). Standard error of pH determination calculated from the variations of the ratios inside of the individual tube did not exceed 0.1 pH units. The averaged ratios calculated from the two phantoms are in good agreement (Fig. 5), with the difference not exceeding 3% for most of points. The calibration data from the two phantoms prepared from 1 mM and 2 mM probe solutions are described by standard titra-

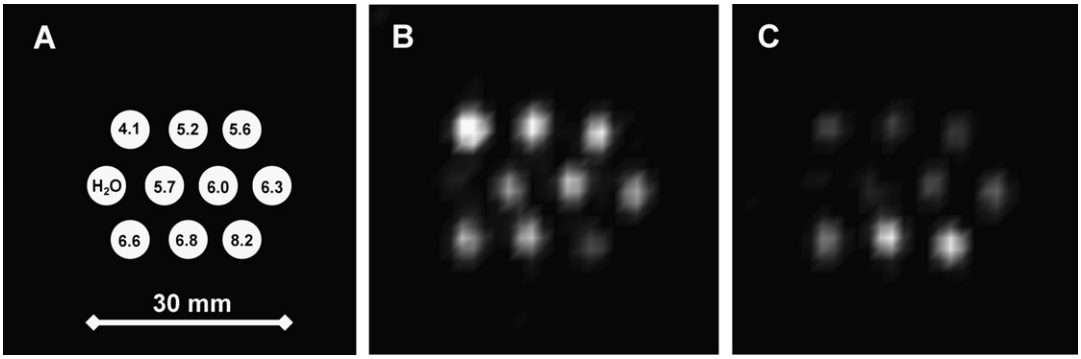

Fig. 4. Calibration of the VRF PEDRI approach for pH mapping. **A**. Schematics of the phantom. White circles represent 10 glass tubes filled with H_2O or 1 mM solutions of the R1 radical titrated to different pH values. Values of pH for each individual tube are shown on the panel. **B**. Image acquired with 560.3 MHz EPR irradiation frequency; **C**. Image acquired with 562.5 MHz EPR irradiation frequency. These frequencies are equally distanced by ±1.12 MHz (±0.4 G) from the central frequency of the resonator, 561.4 MHz. The MRI acquisition parameters are: TR, 500 ms; TE, 19 ms; matrix, 64 × 64; field of view (FOV), 100 × 100 mm; slice thickness, 10 mm; acquisition time, 2.0 s; NMR frequency, 783.3 kHz. EPR irradiation time 2.4 s.

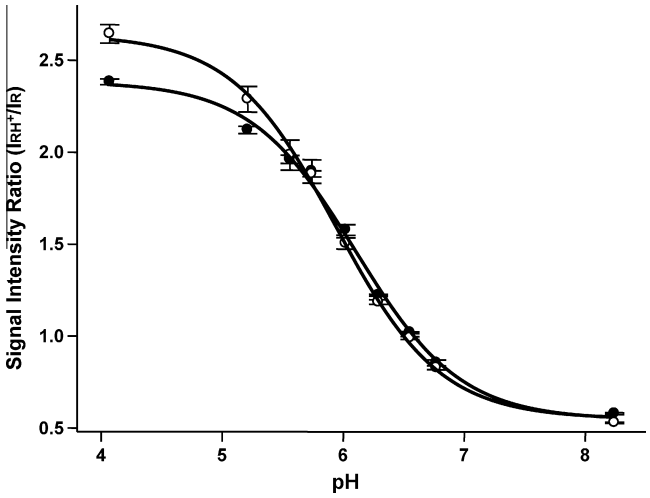

Fig. 5. pH dependence of the ratio of high field VRF PEDRI signal amplitudes acquired at two EPR frequencies, 560.3 and 562.5 MHz. The solid lines are nonlinear least-squares fits of the data to a conventional titration curve, yielding the pK_a values 6.0 (1 mM R1, empty circles) and 6.1 (2 mM R1, filled circles).

tion curves, $I(RF_1)/I(RF_2) = H^+/K_a$, with the close values of the observed pK_a, 6.0 ± 0.1 and 6.1 ± 0.1, respectively. This is in agreement with the previously reported value of pK_a, 6.1, obtained from pH dependence of the hyperfine splitting of the EPR spectra of the radical R1 [15]. Note that pH values accessible for pH mapping using R1 probe and VRF approach are in the range from 5.2 to 6.9.

3.3. pH mapping aqueous samples using VRF PEDRI: phantom mimicking small animal object

To simulate a mouse body resonator load, a phantom was constructed from 35 mm long plastic tube with a 29 mm diameter which was tightly packed with open-ended thin wall glass tubes and filled with 23 ml of 7.5 mM NaCl solution. Two tubes, 4 mm long and 5 mm of inner diameter, filled with 80 μl of 1 mM R1 solutions at pH 6.1 and 6.4, were placed into the phantom simulating local introduction of the probe in the mouse body. The images of this phantom, taken at EPR frequencies RF_1 and RF_2, and magnetic field as those used for calibration, are shown in Fig. 6A and 6B. The pH map shown in Fig. 6C was constructed from the ratios of Overhauser-enhanced MRI signals at each pixel of the images 6A and 6B using a calibration curve (Fig. 5). The obtained functional image, pH map, required three acquisitions, one EPR *off* and two EPR *on*, with total acquisition time of 6.8 s and EPR RF irradiation time of 4.8 s, shows spatial resolution of 1.56 mm and functional resolution of about 0.1 pH units.

4. Discussion

Recently we demonstrated that VF PEDRI allows specific functional information to be obtained along with spatial information on the structure of the object and the distribution of the radical

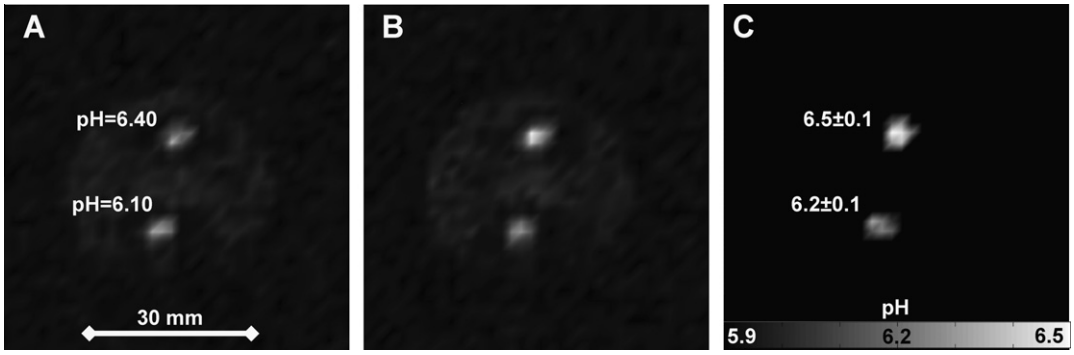

Fig. 6. pH mapping of the mouse-mimicking phantom using VRF PEDRI. **A**, **B**, images of a phantom mimicking mouse with two local infusions of pH-sensitive probe. Two tubes, 4 mm long and 5 mm of inner diameter, filled with 80 μl of 1 mM R1 solutions at pH 6.1 and 6.4, are placed into bigger tube filled with saline solution. Images were acquired using two EPR frequencies, 560.3 MHz (**A**) and 562.5 MHz (**B**), MRI acquisition parameters: TR, 500 ms; TE, 19 ms; matrix, 64 × 64; FOV, 100 × 100 mm; slice thickness, 10 mm; acquisition time, 2 s; EPR irradiation time 2.4 s, NMR frequency, 783.3 kHz. **C**. pH map of the phantom constructed from the ratios of Overhauser-enhanced MRI signals at each pixel of the images **A** and **B** using a calibration curve. The values of pH averaged over each tube are indicated on the panel.

within the object [12]. Using this approach the functional image of the aqueous sample, e.g. pH map, can be extracted from the value of the enhancements observed at each pixel of the PEDRI images acquired after EPR irradiation of a pH-sensitive probe at two preselected magnetic fields. Variations in magnetic field in VF PEDRI experiments resulted in relatively long field stabilization times and, as a consequence, long acquisition times of about one minute using a gradient echo pulse sequence [12].

An alternative approach termed variable radio frequency (VRF) PEDRI with a stationary magnetic field but slightly different EPR radio frequencies was proposed for functional mapping using specific paramagnetic probes. This approach requires minimal instrumental modification of the fixed-field PEDRI system. Modification requires inclusion of either a dual-frequency switchable resonator or a wide-band resonator for EPR irradiation at close frequencies. Compared with the variable field approach, VRF PEDRI improves magnetic field homogeneity and stability and decreases acquisition time by eliminating periods of ramping and stabilization of the magnetic field.

In this work accurate VRF measurements were performed using an existing PEDRI setup with a modified Alderman–Grant resonator [14]. Future development of a simplified VRF PEDRI system may allow for elimination of the field cycling coil and its power supplies, an increased gap in the magnet system, and the possibility to use conventional NMR gradients and gradient power supplies. High stability of the magnetic field during proton MRI acquisition in the VRF PEDRI set up facilitated application of the fast spin echo sequence. This resulted in decreasing the acquisition time by about 30-fold to 2.4 s (Fig. 4) down from about one minute in the case of VF PEDRI [12], therefore reducing crucial problems of sample heating and probe instability in vivo. A modified Alderman–Grant resonator has a Q factor about 200 when loaded with a sample allowing for acquiring reliable images at two EPR frequencies distanced from each other up to 3.4 MHz (equivalent to 1.2 G). Larger separation moves the frequencies further away from the resonance frequency of the resonator and reduces its efficiency. This fact limits the applicability of the method to the probes with EPR spectral features separated by less or about 1.2 G. pH-sensitive imidazoline nitroxides are examples of probes with the differences in nitrogen hyperfine splittings between protonated and deprotonated forms of the probe, $\Delta a_N \approx 1$ G (see Fig. 1). In general, a resonator design with a broader band and lower Q factor will allow for use of functional probes with larger separation between characteristic EPR frequencies.

Application of VRF PEDRI to pH mapping of aqueous samples was demonstrated using pH-sensitive imidazoline nitroxide. Stable nitroxides of the imidazoline and imidazolidine types have been proven to be useful pH-sensitive probes for EPR spectroscopy and imaging [12,16,17] due to the large effect of pH on their EPR spectra and the large number of structures synthesized. Fig. 1 illustrates the pH effect on the EPR spectra of one of the imidazoline radicals, R1. Up to the present a wide variety of pH-sensitive nitroxides have been developed with different ranges of pH-sensitivity, labeling groups, lipophilicity and stability towards bioreduction [18–21]. These spin pH probes, together with low field EPR-based techniques, offer unique opportunities for noninvasive pH assessments in living animals in compartments with widely varying pH ranges. The potential applications are enormous, including detection of ischemia-induced acidosis [22], localized reductions in pH in areas of infection or inflammation [23], acidic areas in solid tumors [24], effects of skin treatments on local skin pH at various levels [25] and drug-induced changes in stomach acidity [26]. The acidic extracellular pH in tumors, pH_e, has a number of important consequences, playing a role in tumor initiation, progression, and therapy [24]. Recently, pH_e has been identified as a significant prognostic factor not only in experimental transplantable tumor models but also in spontaneous tumors [27].

The most widely used approach for in vivo pH assessment is based on the pH-sensitivity of ^{31}P NMR shift of endogenous inorganic phosphate, P_i. However pH assessment using ^{31}P NMR has its own limitations, including lack of resolution, chemical shift dependence on ionic strength and inability to report extracellular pH in tumors due to predominant intracellular localization of phosphate [24]. Because of these problems, exogenous NMR probes are being designed to improve detection of myocardial acidosis [28] and extracellular pH in tumors [24,29]. However, application of exogenous paramagnetic pH probes using EPR spectroscopy has the sensitivity and specificity advantage over exogenous NMR probes.

Several studies on application of pH-sensitive nitroxides to pH mapping of aqueous samples using EPR-based techniques have been published in the last decade. pH mapping using spectral–spatial continuous wave (CW) EPRI for phantom samples [23,25,30–32] required long acquisition times (typically >10 min). Data obtained with VF PEDRI demonstrated shortened acquisition times for pH mapping, requiring only a few minutes [12]. Work proposed here using VRF PEDRI makes it possible to further decrease pH mapping acquisition time to a few seconds which is of particular importance for in vivo applications. One potential application includes pH mapping of extracellular pH in tumors. Currently we are utilizing L-band EPR spectroscopy and the imidazoline nitroxide to monitor pH_e in breast cancer tumors in FVB/N female mice [33]. It has been observed that pH_e in tumors is lower than in normal mammary gland tissue by an average of 0.3–0.5 pH units. To demonstrate the potential of VRF PEDRI to map tumor tissue acidosis in vivo we constructed the mouse-mimicking phantom (20 ml aqueous sample with 3 cm diameter) with two small local areas of 80 μl of the nitroxide R1. The areas differed in pH values by 0.3 units. Fig. 6 demonstrates reasonable spatial (1.56 mm) and functional (±0.1 pH units) resolution of the pH map extracted from VRF PEDRI images with a total acquisition time of only 6.8 s. With regard to in vivo pH mapping of tumor tissue acidosis, the membrane impermeable pH-sensitive nitroxide has to be applied to ensure extracellular localization of the probe, e.g. nitroxide R-GSH covalently bound to highly hydrophilic tripeptide, glutathione [33,34]. Unfortunately, GSH-bound nitroxide recently used for tumor pH monitoring [33] has a linewidth about twice as broad as the nitroxide R1. This results in a lower enhancement factor, therefore decreasing functional and spatial image resolution and increasing acquisition time, RF power deposition and sample heating. Upon R1 radical application with linewidth of about 1 G the enhancement factor of about 12 was achieved in the mouse-mimicking phantom, providing reliable reading of signal intensity. The synthesis of the deuterated analogues of pH-sensitive nitroxides, e.g. deuterated R1 and R-GSH, would result in significant decrease of probe linewidth [35], therefore making in vivo pH mapping using VRF PEDRI feasible. Alternative strategy of the development of pH-sensitive probes with narrow EPR linewidths was proposed [36] and is based on the chemical modification of stable trityl radicals. While the first pH-sensitive trityl structures were recently developed [37,38], further work on improvement of their aqueous solubility and spectral properties is required.

Acknowledgments

This work was partly supported by NIH Grants EB009433, EB004900, and CA132068.

References

[1] D.J. Lurie, D.M. Bussell, L.H. Bell, J.R. Mallard, Proton electron double magnetic resonance imaging of free radical solutions, J. Magn. Reson. 76 (1988) 366–370.
[2] K. Golman, I. Leunbach, J.H. Ardenkjaer-Larsen, et al., Overhauser-enhanced MR imaging (OMRI), Acta Radiol. 39 (1) (1998) 10–17.

[3] M.A. Foster, I. Seimenis, D.J. Lurie, The application of PEDRI to the study of free radicals in vivo, Phys. Med. Biol. 43 (1998) 1893–1897.
[4] H. Li, Y. Deng, G. He, P. Kuppusamy, D.J. Lurie, J.L. Zweier, Proton electron double resonance imaging of the in vivo distribution and clearance of a triaryl methyl radical in mice, Magn. Reson. Med. 48 (3) (2002) 530–534.
[5] H. Li, G. He, Y. Deng, P. Kuppusamy, J.L. Zweier, In vivo proton electron double resonance imaging of the distribution and clearance of nitroxide radicals in mice, Magn. Reson. Med. 55 (3) (2006) 669–675.
[6] T. Liebgott, H. Li, Y. Deng, J.L. Zweier, Proton electron double resonance imaging (PEDRI) of the isolated beating rat heart, Magn. Reson. Med. 50 (2) (2003) 391–399.
[7] D.J. Lurie, G.R. Davies, M.A. Foster, J.M. Hutchison, Field-cycled PEDRI imaging of free radicals with detection at 450 mT, Magn. Reson. Imaging 23 (2) (2005) 175–181.
[8] D.J. Lurie, H. Li, S. Petryakov, J.L. Zweier, Development of a PEDRI free-radical imager using a 0.38 T clinical MRI system, Magn. Reson. Med. 47 (1) (2002) 181–186.
[9] H. Utsumi, Yamada Ken-ichi, K. Ichikawa, Kiyoshi Sakai, Y. Kinoshita, S. Matsumoto, M. Nagai, Simultaneous molecular imaging of redox reactions monitored by Overhauser-enhanced MRI with ^{14}N- and ^{15}N-labeled nitroxyl radicals, PNAS 103 (5) (2006) 1463–1468.
[10] D.J. Lurie, J.M.S. Hutchison, L.H. Bell, I. Nicholson, D.M. Bussell, J.R. Mallard, Field-cycled proton–electron double resonance imaging of free radicals in large aqueous samples, J. Magn. Reson. 84 (1989) 431–437.
[11] K. Shet, G. Caia, E. Kesselring, et al., A novel variable field system for field-cycled dynamic nuclear polarization spectroscopy, J. Magn. Reson. 205 (2010) 202–208.
[12] V.V. Khramtsov, G.L. Caia, K. Shet, et al., Variable field proton–electron double-resonance imaging: application to pH mapping of aqueous samples, J. Magn. Reson. 202 (2) (2010) 267–273.
[13] L.B. Volodarsky, I.A. Grigor'ev, Synthesis of heterocyclic nitroxides, in: L.B. Volodarsky (Ed.), Imidazoline Nitroxides, CRC Press, Boca Raton, 1988, pp. 5–28.
[14] S. Petryakov, A. Samouilov, M. Roytenberg, H. Li, J.L. Zweier, Modified Alderman–Grant resonator with high-power stability for proton electron double resonance imaging, Magn. Reson. Med. 56 (3) (2006) 654–659.
[15] V.V. Khramtsov, L.M. Weiner, I.A. Grigor'ev, L.B. Volodarsky, Proton exchange in stable nitroxyl radicals. EPR studies of the pH of aqueous solutions, Chem. Phys. Lett. 91 (1982) 69–72.
[16] V.V. Khramtsov, J.L. Zweier, Functional in vivo EPR spectroscopy and imaging using nitroxide and trityl radicals, in: R. Hicks (Ed.), Stable Radicals: Fundamentals and Applied Aspects of Odd-electron Compounds, John Wiley & Sons, Ltd., 2010, pp. 537–566.
[17] V.V. Khramtsov, I.A. Grigor'ev, M.A. Foster, et al., In vitro and in vivo measurement of pH and thiols by EPR-based techniques, Antioxid. Redox Signal. 6 (3) (2004) 667–676.
[18] V.V. Khramtsov, L.B. Volodarsky, Use of imidazoline nitroxides in studies of chemical reactions. ESR measurements of the concentration and reactivity of protons, thiols and nitric oxide, in: L.J. Berliner (Ed.), Spin Labeling. The next Millennium, Biological Magnetic Resonance, vol. 14, Plenum Press, New York, 1998, pp. 109–180.
[19] I.A. Kirilyuk, A.A. Bobko, I.A. Grigor'ev, V.V. Khramtsov, Synthesis of the tetraethyl substituted pH-sensitive nitroxides of imidazole series with enhanced stability towards reduction, Org. Biomol. Chem. 2 (7) (2004) 1025–1030.
[20] I.A. Kirilyuk, A.A. Bobko, V.V. Khramtsov, I.A. Grigor'ev, Nitroxides with two pK values – useful spin probes for pH monitoring within a broad range, Org. Biomol. Chem. 3 (7) (2005) 1269–1274.
[21] M.A. Voinov, J.F. Polienko, T. Schanding, et al., Synthesis, structure and X-band (9.5 GHz) characterization of the new series of pH-sensitive probes: N-N-disubstituted 4-amino-2, 2,5,5-tetramethyl-3-imidazoline 1 oxyls, J. Org. Chem. 70 (2005) 9702–9711.
[22] J.L. Zweier, P. Wang, A. Samouilov, P. Kuppusamy, Enzyme-independent formation of nitric oxide in biological tissues, Nat. Med. 1 (8) (1995) 804–809.
[23] V.V. Khramtsov, Biological imaging and spectroscopy of pH, Curr. Org. Chem. 9 (2005) 909–923.
[24] R.J. Gillies, N. Raghunand, M.L. Garcia-Martin, R.A. Gatenby, pH imaging. A review of pH measurement methods and applications in cancers, IEEE Eng. Med. Biol. Mag. 23 (5) (2004) 57–64.
[25] C. Kroll, W. Hermann, R. Stosser, H.H. Borchert, K. Mader, Influence of drug treatment on the microacidity in rat and human skin – an in vitro electron spin resonance imaging study, Pharm. Res. 18 (4) (2001) 525–530.
[26] D.I. Potapenko, M.A. Foster, D.J. Lurie, et al., Real-time monitoring of drug-induced changes in the stomach acidity of living rats using improved pH-sensitive nitroxides and low-field EPR techniques, J. Magn. Reson. 182 (1) (2006) 1–11.
[27] M. Lora-Michiels, D. Yu, L. Sanders, et al., Extracellular pH and P-31 magnetic resonance spectroscopic variables are related to outcome in canine soft tissue sarcomas treated with thermoradiotherapy, Clin. Cancer Res. 12 (19) (2006) 5733–5740.
[28] S. Pietri, S. Martel, M. Culcasi, M.C. Delmas-Beauvieux, P. Canioni, J.L. Gallis, Use of diethyl(2-methylpyrrolidin-2-yl)phosphonate as a highly sensitive extra- and intracellular ^{31}P NMR pH indicator in isolated organs. Direct NMR evidence of acidic compartments in the ischemic and reperfused rat liver, J. Biol. Chem. 276 (3) (2001) 1750–1758.
[29] R.J. Gillies, Z. Liu, Z. Bhujwalla, 31P-MRS measurements of extracellular pH of tumors using 3-aminopropylphosphonate, Am. J. Physiol. 267 (1 Pt. 1) (1994) C195–C203.
[30] A. Sotgiu, K. Mader, G. Placidi, S. Colacicchi, C.L. Ursini, M. Alecci, PH-sensitive imaging by low-frequency EPR: a model study for biological applications, Phys. Med. Biol. 43 (7) (1998) 1921–1930.
[31] V.V. Khramtsov, I.A. Grigor'ev, M.A. Foster, D.J. Lurie, J.L. Zweier, P. Kuppusamy, Spin pH and SH probes: enhancing functionality of EPR-based techniques, Spectroscopy 18 (2004) 213–225.
[32] K. Mader, S. Nitschke, R. Stosser, H.H. Borchert, Non-destructive and localized assessment of acidic microenvironments inside biodegradable polyanhydrides by spectral spatial electron paramagnetic resonance imaging, Polymer 38 (19) (1997) 4785–4794.
[33] A.A. Bobko, I.A. Kirilyuk, T.D. Eubank, et al., In vivo extracellular pH monitoring in tumor tissues of PyMT mice: effect of GM-CSF treatment, Free Radical Biol. Med. 47 (Suppl. 1) (2009) S166.
[34] Y.Y. Woldman, S.V. Semenov, A.A. Bobko, et al., Design of liposome-based pH sensitive nanoSPIN probes: nano-sized particles with incorporated nitroxides, Analyst 134 (2009) 904–910.
[35] Y.I. Glazachev, I.A. Grigor'ev, E.J. Reijerse, V.V. Khramtsov, EPR studies of ^{15}N- and ^{2}H-substituted pH-sensitive spin probes of imidazoline and imidazolidine types, Appl. Magn. Reson. 20 (2001) 489–505.
[36] A.A. Bobko, I. Dhimitruka, J.L. Zweier, V.V. Khramtsov, Trityl radicals as persistent dual function pH and oxygen probes for in vivo electron paramagnetic resonance spectroscopy and imaging: concept and experiment, J. Am. Chem. Soc. 129 (23) (2007) 7240–7241.
[37] I. Dhimitruka, A.A. Bobko, C.M. Hadad, J.L. Zweier, V.V. Khramtsov, Synthesis and characterization of amino derivatives of persistent trityl radicals as dual function pH and oxygen paramagnetic probes, J. Am. Chem. Soc. 130 (32) (2008) 10780–10787.
[38] Y. Liu, F.A. Villamena, J.L. Zweier, Highly stable dendritic trityl radicals as oxygen and pH probe, Chem. Commun. (Camb) (36) (2008) 4336–4338.